

# Flat-band many-body localization in the Creutz ladder

Yoshihito Kuno\*

*Department of Physics, Graduate School of Science, Kyoto University, Kyoto 606-8502, Japan*

Takahiro Orito\* and Ikuo Ichinose

*Department of Applied Physics, Nagoya Institute of Technology, Nagoya, 466-8555, Japan*

(Dated: April 16, 2019)

Study on a disorder-free many-body localization is reported for the flat-band Creutz ladder, which was recently realized in cold-atoms in an optical lattice. In a non-interacting case, the flat-band structure leads to a Wannier wavefunction localized on four adjacent lattice sites. In the flat-band regime both with and without interactions, the level spacing analysis exhibits Poisson-like distribution. This indicates the existence of the disorder-free localization. Calculation of the inverse participation ratio supports this observation. Interestingly, this type of localization is robust to weak disorders, whereas for strong disorders, the system exhibits a crossover into the conventional disorder-induced many-body localization phase. We also find non-ergodic dynamics in the flat-band regime without disorder. The memory of an initial density wave pattern is preserved for long times.

*Introduction.*— Localization and absence of diffusion in non-interacting electron systems have been extensively studied since Anderson discussed the disorder effect in solids on the single-particle electron wavefunction [1]. Presently, what is called the Anderson localization (AL), is recognized as a universal phenomenon in various physical systems [2]. In AL quantum systems, a single-particle electron wavefunction is exponentially localized with a localization length, which leads to a type of insulating phase. Owing to the recent development in the computational power and numerical techniques, study on the effect of the interactions between particles on the AL is currently one of the main research topics in condensed matter physics. It is now recognized that the AL persists in some cases even if the particles interact. This is the so-called many-body localization (MBL). Mostly by numerical simulations, it has been clarified that the MBL phase exhibits some characteristic properties such as Poisson distribution in the level spacing analysis (LSA) of the energy eigenvalues similar to that of the conventional AL and the logarithmic growth of entanglement entropy. In its glassy dynamics, MBL is closely related with the breaking of eigenstate thermalization hypothesis and ergodicity breaking dynamics [3–7]. Recent experiments on cold-atom gases in optical lattices have reported evidences for the existence of MBL phenomena [8, 9].

Until recently, most of the theoretical studies have focused on MBL induced by the disorders encoded in the on-site potentials, hopping amplitudes and interactions, as well as quasi-periodic potentials [10]. Contrastingly, extremely recently, disorder-free AL/MBL-like phenomena have been revealed in a Wannier–Stark ladder [11, 12], dipolar atom gases in an optical lattice [13], some lattice-gauge theoretical models [14–17], quantum Hall systems [18], a diamond chain system [19–21], and a disorder-free spin chain [22–25]. Motivated by these discoveries, we shall report another type of disorder-free MBL system in this letter. It is a flat-band

system with interactions. The flat-band structure suppresses particle hopping effectively and generates a localized Wannier state [26, 27] similar to the conventional localized wavefunction in the conventional AL system. We are motivated by the existence of such localized wavefunctions and study a flat-band type localization in the Creutz ladder [28]. The Creutz ladder is a simple model and also experimentally feasible in cold atom gases. So far, there are several theoretical proposals for implementation of the model [29–32] and several experimental realizations of related models [33–35]. Thus, the physical properties of the model have been extensively studied [36–38]. We perform the LSA with weak disorders under the flat-band condition and find that the probability distribution exhibits Poissonian behavior for both the non-interacting and interacting cases, indicating a localization tendency. The inverse participation ratio (IPR) also supports the localization tendency. Furthermore, we find that the dynamics in the flat-band Creutz ladder exhibits ergodicity breaking dynamics, i.e., the memory of the particle distribution in initial states is preserved for long times.

*Creutz ladder model.*— In this work, we study an interacting Creutz ladder with the Hamiltonian [28],

$$\begin{aligned} H = \sum_j & \left[ -it_1(a_{j+1}^\dagger a_j - b_{j+1}^\dagger b_j) - t_0(a_{j+1}^\dagger b_j + b_{j+1}^\dagger a_j) + \text{h.c.} \right. \\ & + V(n_{a,j}n_{a,j+1} + n_{b,j}n_{b,j+1} + n_{a,j}n_{b,j+1} + n_{b,j}n_{a,j+1}) \\ & \left. + \mu_{a,j}n_{a,j} + \mu_{b,j}n_{b,j} \right], \end{aligned} \quad (1)$$

where  $a_j^{(\dagger)}$  and  $b_j^{(\dagger)}$  are the fermion annihilation (creation) operators on the upper and lower chains, respectively, and subscript  $j$  denotes a unit cell.  $n_{a(b),j}$  is the number operator of the particle on the upper (lower) chain.  $t_1$  and  $t_0$  are the intra-chain and inter-chain hopping amplitudes, respectively.  $V$  is the intra-chain and inter-chain repulsions, as depicted in Fig. 1 (a).  $\mu_{a(b),j}$  is a ran-

dom disorder chemical potential, which has a uniform distribution, such as  $\mu_{a(b),j} \in [-\mu/2, \mu/2]$ . The model is feasible in recent experiments by using a synthetic dimensional method [33, 34] or spin-dependent lattice with lattice modulation technique [35].

The energy spectrum of the non-interacting case of  $H$  in Eq. (1), with  $V = \mu = 0$  is given as  $E(k) = \pm\sqrt{(2t_1 \sin k)^2 + (2t_0 \cos k)^2}$ , where  $k$  is the wave number and the bandwidth is  $|2(t_1 - t_0)|$ . As shown in Figs. 1 (b) and (c), the band is flat for  $t_1 = t_0$  with  $E(k) = -2t_1$ , whereas it is dispersive for  $t_1 \neq t_0$ . The non-interacting case of  $H$  in Eq. (1), with  $\mu = 0$  belongs to the BDI or AIII class in the topological classification theory [39, 40]. This symmetry affects the spectrum distribution of the system. In particular, the chiral symmetry makes the energy spectrum symmetric around zero energy. In addition, at the flat-band point,  $t_0 = t_1$ , a localized Wannier state exists in the system, whose wavefunction is given by [26, 27]

$$|\Psi_w\rangle = -\frac{1}{2} \left[ ia_j^\dagger + a_{j+1}^\dagger + b_j^\dagger + ib_{j+1}^\dagger \right] |0\rangle, \quad (2)$$

where  $|0\rangle$  is the empty state. The state  $|\Psi_w\rangle$  spans over two adjacent unit cells, i.e., it is a four-site localized state. We will subsequently show that this state is a key ingredient for appearance of a new type of localized states.

Here, we note that in the conventional AL, disorder causes localized states to substantially reside on a *single lattice site*. Contrastingly in the flat-band case, the target Wannier state has finite components in a finite region with *multiple lattice sites*. In the Creutz ladder case, the number of sites is four, as shown in Eq. (2). [See also Fig. 1 (a).] It will be subsequently explained that this fact introduces certain constraints on the set-up of an initial state for observing MBL dynamics.

*Level spacing analysis and IPR.*— To investigate the localization properties of the present model, we first perform the LSA by full-diagonalization of the Hamiltonian  $H$  in Eq.(1), under the periodic boundary condition. In the LSA, we employ the usual unfolding analysis [41] to obtain a clear probability distribution of the level spacing of the energy eigenvalues. Here, our interest is in the disorder-free and weak-disorder regimes. In performing the LSA for the disorder-free case ( $\mu = 0$ ), it is important to note that the system has the translational symmetry. This symmetry generally leads to numerous degeneracies in the energy eigenvalues. Because of the degeneracies, it is not simple to obtain the probability distributions of the level spacing without ambiguities [11, 12]. To avoid this difficulty, we consider the cases with small but finite disorders. In the presence of disorders, even those that are extremely weak, the degeneracies of the energy eigenvalues are solved, and subsequently, we can obtain a clear probability distribution of the level spacing, which substantially captures the characteristics of the disorder-free system. In practical calculations, we consider the

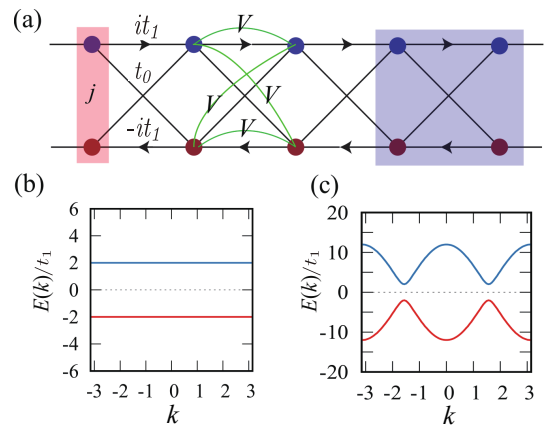


FIG. 1: (a) Creutz ladder: the red shaded area represents a unit cell and the blue one is a Wannier state under the flat-band condition,  $t_1 = t_0$ . (b) Flat-band structure at  $t_0 = t_1$ . (c) Dispersive (non-flat-band) band structure at  $t_0 = 6t_1$ .

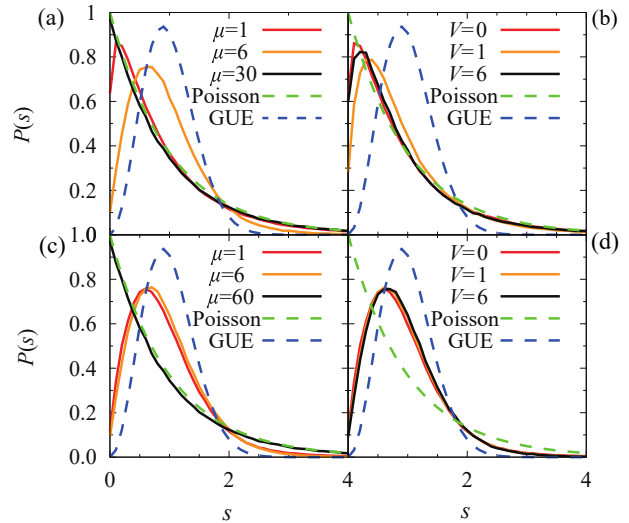


FIG. 2: Level spacing analysis: (a) Disorder dependence in non-interacting flat-band ( $V = 0$ ). (b) Interaction dependence in disordered flat-band ( $\mu = 1$ ). (c) Disorder dependence in non-interacting non-flat-band ( $V = 0$ ). (d) Interaction dependence in disordered non-flat-band ( $\mu = 1$ ).

upper and lower chains with length  $L = 16$  and number of particle  $N = 4$  (i.e., the filling factor is  $1/8$ ). The Hilbert space dimension expanded by the Fock state is 35960, and we discard the top and bottom 10% of the energy eigenvalues to obtain a clear distribution. From the LSA, we examine the localization properties of the system. In general, for an ensemble of localized states, the probability distribution exhibits Poisson statistics, such as  $P_P(s) \propto \exp(-s)$ , where  $s$  denotes the unfolded level spacing. Contrastingly, for an ensemble of delocalized (extended) states, the probability distribution is to

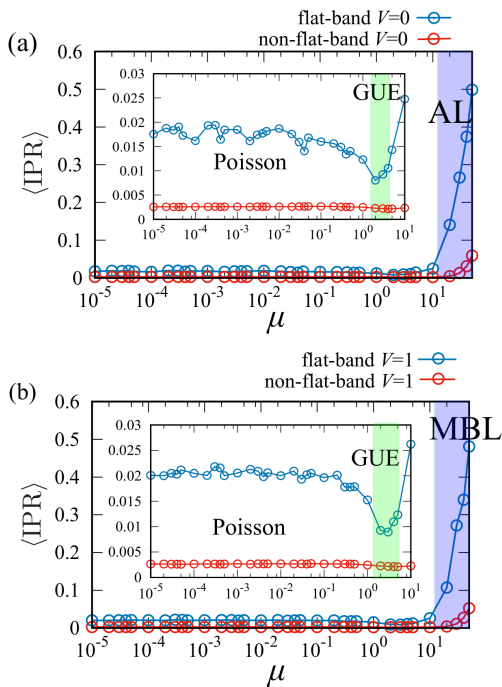


FIG. 3: Disorder dependence of the averaged IPR: (a) Non-interacting case ( $V = 0$ ). (b) Interacting case ( $V = 1$ ). For both the cases, we averaged over 20 disorder samples. In the weak-disorder regime ( $\mu < 1$ ), there exists a large difference in the value of the IPR of the flat-band and non-flat-band. In both cases (a) and (b), the difference becomes small for  $1 \lesssim \mu \lesssim 10$ , where the LSA of the flat-band exhibits GUE-like distribution. In the  $\mu \gtrsim 10$  regime, the averaged IPR increases rapidly. This indicates the existence of a crossover to the conventional disorder-induced AL/MBL phase. The system size is  $L = 12$ , and the particle number is  $N = 3$ .

be Gaussian unitary ensemble (GUE), with characteristics such as  $P_G(s) \propto s^2 \exp(-4s^2/\pi)$  [6, 7, 42–49].

Figure 2 (a) shows the obtained probability distribution for various disorder strengths for the non-interacting flat-band ( $V = 0$ ,  $t_1 = t_0$ ). We find that for a weak disorder ( $\mu = 1$ ), the probability distribution is extremely similar to Poisson statistics. This result indicates the existence of localized states even in a weak disorder. With increasing disorder strength, we observe an interesting phenomenon, i.e., first, the statistics changes from Poisson to GUE-like, and then it returns to the Poisson statistics. Calculations for  $\mu = 6$  and  $\mu = 30$  shown in Fig. 2 (a) clearly exhibit this behavior: Poisson  $\rightarrow$  GUE  $\rightarrow$  Poisson. The above behavior of the Creutz ladder model is somewhat different from the flat-band models studied in Refs. [47, 48]. We understand our findings as follows. The Poisson statistics for the  $\mu = 30$  ensemble originates from the conventional AL that is induced by disorder. Contrastingly, the Poisson-like statistics for the  $\mu = 1$  ensemble arises from the flat-band properties of the model. Crossover takes place from the

flat-band localization to the disorder-induced AL as the disorder increases [50]. This conclusion is subsequently supported by the IPR calculation.

Figure 2 (b) shows the LSA of the interacting cases with a weak disorder,  $\mu = 1$ . We find that even for finite interactions  $V = 1$  and 6, the Poisson-like statistics persists. This result is indicative of the disorder-free MBL induced by the flat-band structure.

We also study the non-flat-band case ( $t = 6t_0$ ), which we regard as a reference system with respect to the AL in finite-size systems. Figure. 2 (c) shows the LSA of a non-interacting non-flat-band for various  $\mu$ 's. The  $\mu = 1$  and  $\mu = 6$  results are close to GUE, whereas for a larger disorder,  $\mu = 60$ , the conventional disorder-induced AL occurs. This delocalization-like behavior is robust to the interaction, as shown in Fig. 2 (d). The obtained result, in particular for the non-interacting case, seems to contradict the common belief that all the states are localized in 1D random-potential systems. Probably, this is a finite-size effect [51], i.e., for a weak disorder,  $\mu = 1$ , localization lengths of certain part of states are larger than the system size. By comparing the results in Figs. 2 (a) and (b) with those in Figs. 2 (c) and (d), we find that the localization in the flat-band is stronger than that in the non-flat-band, indicating that their mechanisms are different. We will confirm this inference by calculating other quantities.

We calculate the IPR, which is often used for the study of localization. By diagonalizing the Hamiltonian in Eq. (1), we obtain all the eigenvectors,  $|\psi_\ell\rangle = \sum_m c_m^\ell |F_m\rangle$ , where  $\ell$  labels the eigenstates,  $|F_m\rangle$  is the Fock-state base and  $\{c_m^\ell\}$  are the coefficients. For these eigenstates, the IPR is defined as

$$(\text{IPR})_\ell = \sum_m |c_m^\ell|^4. \quad (3)$$

In particular for a non-interacting system with  $N$  particles,  $(\text{IPR})_\ell$  in Eq. (3) is related to the localization length,  $R_\ell$  [in units of the lattice spacing], because  $(\text{IPR})_\ell \simeq 1/(R_\ell)^N$  [17]. In this work, we average  $(\text{IPR})_\ell$  over all the states for fixed  $\mu$  and  $V$ . The averaged IPR is denoted by  $\langle \text{IPR} \rangle$ .

Figure 3 (a) shows the  $\mu$ -dependence of  $\langle \text{IPR} \rangle$  in the non-interacting case ( $V = 0$ ). For a sufficiently weak disorder ( $\mu \lesssim 1$ ), the obtained  $\langle \text{IPR} \rangle$  in both the flat-band ( $t_0 = t_1$ ) and non-flat band ( $t_0 = 6t_1$ ) is small compared with that in the strong-disorder regime ( $\mu \gtrsim 10$ ), where the value of  $\langle \text{IPR} \rangle$  is large owing to the existence of the conventional disorder-induced AL. In the weak-disorder regime, there exists a clear difference in the  $\langle \text{IPR} \rangle$  of the flat-band and non-flat-band cases [52], i.e., the value of the  $\langle \text{IPR} \rangle$  of the flat-band is obviously much larger than that of the non-flat-band system. A simple estimation of the average of  $R_\ell$ ,  $\langle R \rangle$  by using  $\langle \text{IPR} \rangle$  yields  $\langle R \rangle \simeq 8$

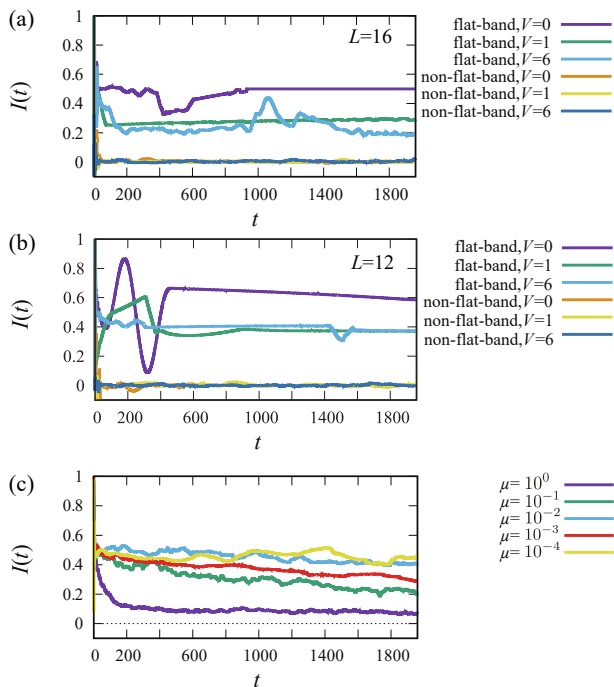


FIG. 4: Time evolution of the imbalance,  $I(t)$ : (a)  $L = 16$  disorder-free case. (b)  $L = 12$  disorder-free case. (c) Disorder dependence for the interacting flat-band case ( $V = 1$ ). We averaged over 50 disorder samples. In all the flat-band cases,  $I(t)$  shows a nontrivial behavior and maintains a non-vanishing value at  $t = 2000$ . Contrastingly, in the non-flat-band cases,  $I(t)$  rapidly decreases to zero.

for the non-flat-band and  $\langle R \rangle \simeq 4$  for the flat-band. This result for the flat-band,  $\langle R \rangle \simeq 4$ , is reminiscent of the Wannier state in Eq. (2).

It is interesting to observe that in the vicinity  $\mu \sim 6$ ,  $\langle \text{IPR} \rangle$  decreases in the flat-band system, as shown in the inset of Fig. 3 (a). This behavior is in good agreement with the result of the LSA presented in Fig. 2 (a). In fact for  $\mu = 6$ , the LSA of the flat-band shows a GUE-like behavior. Again this behavior of  $\langle \text{IPR} \rangle$  is an evidence of the crossover.

As our main concern is the MBL state in the flat-band, we study the interacting cases with finite  $V$ 's. Calculations of the IPR for the case,  $V = 1$ , are shown in Fig. 2 (b). We find that the value of  $\langle \text{IPR} \rangle$  of the flat-band increases in the weak-disorder regime compared with the  $V = 0$  case, and it again decreases considerably near  $\mu \sim 6$  as in the  $V = 0$  case. We investigated cases for other values of  $V$  and found similar behavior of  $\langle \text{IPR} \rangle$ . We, therefore, conclude that *MBL exists in the flat-band Creutz ladder model in the weak-disorder regime, reflecting the flat-band structure. Moreover, a crossover from flat-band MBL to disorder-induced MBL takes place as the disorder increases.* This is one of the main conclusions of this work.

*Localization dynamics.*— The above results of the LSA

and IPR indicate that disorder-free AL and MBL occur in the flat-band Creutz ladder. This motivates us to simulate the dynamics of the Creutz ladder system. In the conventional disorder-induced AL and MBL, information of an initial density wave pattern is stored for long times [3–6]. This behavior is a hallmark of ergodicity breaking and indicates the breaking of the eigenstate thermalization hypothesis [3, 53]. Here, we focus on the disorder-free and weak-disorder cases and investigate whether the flat-band Creutz ladder exhibits ergodicity breaking dynamics. To this end, we employ the Krylov subspace dynamical method [54, 55] and observe the time evolution of an initially prepared density-wave pattern that is not entangled.

As a technical problem, the Lanczos algorithm for the temporal evolution of the quantum states does not preserve the orthogonality of the Krylov subspace vectors, and this causes deviations from the correct evolution of the system [11, 56]. To solve this problem, we employ the QR decomposition [56], which preserves the orthogonality of the Krylov subspace vectors during time evolution [57].

We simulate the time evolution of an initial state such as  $|\psi_{ini}\rangle = \sum_{i=1}^{L/4} a_{4i-3}^\dagger |0\rangle$ . This density pattern is suitable for detecting the localization dynamics because the Wannier state is localized over four sites in the flat-band regime, as shown in Fig. 1 (a). As an indicator of ergodicity breaking dynamics, we introduce the particle imbalance,  $I(t)$ , defined as

$$I(t) = \frac{N_o - N_e}{N_o + N_e}, \quad (4)$$

where  $N_o \equiv \sum_{i=1}^{L/4} \sum_{\alpha=a,b} (n_{\alpha,4i-3} + n_{\alpha,4i-2})$  and  $N_e \equiv \sum_{i=1}^{L/4} \sum_{\alpha=a,b} (n_{\alpha,4i-1} + n_{\alpha,4i})$ . If the value of  $I(t)$  is finite, the memory of the initial state is preserved. This implies there is ergodicity breaking. In the numerical calculation, we set the unit of time as  $\hbar/t_1$ , and use the time slice,  $dt = 10^{-2}$ . Figures 4 (a) and (b) show the time evolution of  $I(t)$  in the disorder-free case ( $\mu = 0$ ) for  $L = 16$  and  $L = 12$  with filling  $1/8$ , respectively. The results for the  $L = 16$  and  $L = 12$  cases exhibit similar behaviors. For  $V = 0$ , the imbalance,  $I(t)$ , for the flat-band maintains a finite value for long times, whereas  $I(t)$  for the non-flat-band instantaneously drops to zero. The above result indicates that the flat-band structure leads to an extremely slow relaxation of the initial state and causes an ergodicity breaking mechanism.

From Figs. 4 (a) and (b), it is obvious that the above behavior of  $I(t)$  is preserved in the presence of interactions. We conclude that a disorder-free MBL exists in the flat-band Creutz ladder both with and without interactions, and *it exhibits ergodicity breaking dynamics.*

We also calculated  $I(t)$  for finite-disorder flat-band cases, as shown in Fig. 4 (c). The result indicates that the disorder-free localization dynamics is robust to at least

weak disorders. This behavior is consistent with the results of the LSA as shown in Fig. 2, and IPR in Fig. 3. The maintenance of the finite value of  $I(t)$  for long times is related to the Poisson-like distribution in the LSA and relatively large IPR compared to that of the AL in the non-flat-band. The results for the strong-disorder cases are provided in the Supplemental Material [51].

*Conclusion.*— We clarified disorder-free AL and MBL phenomena induced by the flat-band structure in the Creutz ladder model with interactions. In the flat-band system, the LSA exhibits Poisson distribution in the weak-disorder regime for both the free and interacting cases. This result indicates the existence of disorder-free AL and MBL phases in the Creutz ladder. We calculated the IPR and found that it supports this result. Furthermore, we performed dynamical simulations. We designed a suitable density pattern as an initial state, simulated the system dynamics, and measured the particle imbalance in the flat-band Creutz ladder. We found an ergodicity-breaking dynamics similar to the conventional disorder-induced AL and MBL dynamics. This behavior is robust to weak disorders. The measurement of particle imbalance is feasible in recent experiments [33, 35], and we believe that our findings will be confirmed in the near future. We also expect that phenomena similar to our findings will be observed in other types of flat-band models, such as the saw-tooth lattice and Lieb lattice models, which are to be realized by cold-atoms [58, 59] or photonic crystals [60, 61].

*Acknowledgments.*— Y. K. acknowledges the support of the Grant-in-Aid for JSPS Fellows (No.17J00486).

---

\* These two authors contributed equally.

- [1] P. W. Anderson, *Phys. Rev.* **109** 1492 (1958).
- [2] A. Lagendijk, B. Van Tiggelen, and D. S. Wiersma, *Phys. Today* **62**, 24 (2009).
- [3] R. Nandkishore and D. A. Huse, *Annu. Rev. Condens. Matter Phys.* **6**, 15 (2015).
- [4] D. M. Basko, I. L. Aleiner, and B. L. Altshuler, *Ann. Phys.* **321**, 1126 (2006).
- [5] D. A. Abanin and Z. Papic, *Annalen der Physik* **529**, 1700169 (2017).
- [6] F. Alet and N. Laflorencie, *Comptes Rendus Physique* **19**, 498 (2018).
- [7] V. Oganesyan and D. A. Huse, *Phys. Rev. B* **75**, 155111 (2007).
- [8] M. Schreiber, S. S. Hodgman, P. Bordia, H. P. Luschen, M. H. Fischer, R. Vosk, E. Altman, U. Schneider, and I. Bloch, *Science* **349**, 842 (2015).
- [9] J.-Y. Choi, S. Hild, J. Zeiher, P. Schaus, A. Rubio-Abadal, T. Yefsah, V. Khemani, D. A. Huse, I. Bloch, and C. Gross, *Science* **352**, 1547 (2016).
- [10] S. Iyer, V. Oganesyan, G. Refael, and D. A. Huse, *Phys. Rev. B* **87**, 134202 (2013).
- [11] E. P. L. van Nieuwenburg, Y. Baum, and G. Refael, arXiv: 1808.00471 (2019).
- [12] M. Schulz, C. A. Hooley, R. Moessner, and F. Pollmann, *Phys. Rev. Lett.* **122**, 40606 (2019).
- [13] W. Li, A. Dhar, X. Deng, K. Kasamatsu, L. Barbiero, and L. Santos, arxiv: 1901.09762 (2019).
- [14] A. Smith, J. Knolle, D. L. Kovrizhin, and R. Moessner, *Phys. Rev. Lett.* **118**, 266601 (2017).
- [15] A. Smith, J. Knolle, R. Moessner, and D. L. Kovrizhin, *Phys. Rev. Lett.* **119**, 176601 (2017).
- [16] M. Brenes, M. Dalmonte, M. Heyl, and A. Scardicchio, *Phys. Rev. Lett.* **120**, 030601 (2018).
- [17] T. Takaiishi, K. Sakakibara, I. Ichinose, and T. Matsui, *Phys. Rev. B* **98**, 184204 (2018).
- [18] A. Krishna, M. Ippoliti, and R. N. Bhatt, *Phys. Rev. B* **99**, 041111(R) (2019).
- [19] J. Vidal, B. Doucot, R. Mosseri, and P. Butaud, *Phys. Rev. Lett.* **85**, 3906 (2000).
- [20] B. Douçot and J. Vidal, *Phys. Rev. Lett.* **88**, 227005 (2002).
- [21] C. Cartwright, G. De Chiara, and M. Rizzi, *Phys. Rev. B* **98**, 184508 (2018).
- [22] M. Kormos, M. Collura, G. Takacs, and P. Calabrese, *Nat. Phys.* **13**, 246 (2017).
- [23] P. P. Mazza, G. Peretto, A. Leroose, M. Collura, A. Gambassi, arxiv: 1806.09674 (2018).
- [24] F. Liu, R. Lundgren, P. Titum, G. Pagano, J. Zhang, C. Monroe, A. V. Gorshkov, arxiv: 1810.02365 (2018).
- [25] A. Leroose, B. Zunkovic, A. Silva, A. Gambassi, *Phys. Rev. B* **99** 121112 (2019).
- [26] S. Takayoshi, H. Katsura, N. Watanabe, and H. Aoki, *Phys. Rev. A* **88**, 063613 (2013).
- [27] R. Mondaini, G. G. Batrouni, and B. Gremaud, *Phys. Rev. B* **98**, 155142 (2018).
- [28] M. Creutz, *Rev. Mod. Phys.* **73**, 119 (2001).
- [29] A. Bermudez, L. Mazza, M. Rizzi, N. Goldman, M. Lewenstein, and M. A. Martin-Delgado, *Phys. Rev. Lett.* **105** 190404 (2010).
- [30] L. Mazza, A. Bermudez, N. Goldman, M. Rizzi, M. A. Martin-Delgado, and M. Lewenstein, *New. J. Phys.* **14**, 015007 (2012).
- [31] J. Junemann, A. Piga, S. Ran, M. Lewenstein, M. Rizzi, and A. Bermudez, *Phys. Rev. X* **7**, 031057 (2017).
- [32] Y. Kuno, I. Ichinose and Y. Takahashi, *Sci. Rep.* **8**, 10699 (2018).
- [33] M. Mancini, G. Pagano, G. Cappellini, L. Livi, M. Rider, J. Catani, C. Sias, P. Zoller, M. Inguscio, M. Dalmonte, and L. Fallani, *Science* **349**, 1510 (2015).
- [34] A. Celi, P. Massignan, J. Ruseckas, N. Goldman, I. B. Spielman, G. Juzeliunas, and M. Lewenstein, *Phys. Rev. Lett.* **112**, 043001 (2014).
- [35] J. H. Kang, H. Han, and Y. Shin, arXiv:1902.10304 (2019).
- [36] A. Bermudez, D. Patanè, L. Amico, and M. A. Martin-Delgado, *Phys. Rev. Lett.* **102**, 135702 (2009).
- [37] D. Gonzalez-Cuadra, A. Dauphin, P. R. Grzybowski, P. Wójcik, M. Lewenstein, and A. Bermudez, *Phys. Rev. B* **99**, 045139 (2019).
- [38] E. Tirrito, M. Rizzi, G. Sierra, M. Lewenstein, and A. Bermudez, *Phys. Rev. B* **99**, 125106 (2019).
- [39] A. P. Schnyder, S. Ryu, A. Furusaki, and A. W. W. Ludwig, *Phys. Rev. B* **78**, 195125 (2008).
- [40] A. Kitaev, in *Advances in Theoretical Physics: Landau Memorial Conference*, edited by V. Lebedev and M. Feiguelfman, AIP Conf. Proc. No. 1134 (AIP, Melville, NY, 2009), p. 22.

- [41] L. F. Santos, and M. Rigol, Phys. Rev. E **81**, 036206 (2010).
- [42] E. Abrahams et al. Phys. Rev. Lett., **42**, 673 (1979).
- [43] H. Grussbach, M. Schreiber, Phys. Rev. B **51**, 663 (1995).
- [44] S. Hikami, Phys. Rev. B **24**, 2671 (1981).
- [45] K. B. Efetov, A. I. Larkin, D. E. Khmel'nitsukii, JETP **52**, 568 (1980).
- [46] K. B. Efetov, "Supersymmetry in Disorder and Chaos", Cambridge Univ. Press (1977).
- [47] J. T. Chalker, T. S. Pickles, and P. Shukla, Phys. Rev. B **82**, 104209 (2010).
- [48] P. Shukla, Phys. Rev. B **98**, 184202 (2018).
- [49] The probability distribution is not Gaussian orthogonal ensemble because our Hamiltonian matrix is not real-symmetric but only Hermitian.
- [50] Similar recurrence phenomenon of the glassy dynamics by disorder strength was observed recently for an extended Bose–Hubbard model, which is a quantum simulator of the lattice gauge–Higgs model. J. Park, Y. Kuno, and I. Ichinose, arXiv: 1903.07297.
- [51] Supplemental material:
- [52] The small values of  $\langle \text{IPR} \rangle$  are partly owing to the degeneracy originating from the translational symmetry of the model. In the small-disorder regime, the breakdown of the translational symmetry is weak. Accordingly, there exist numerous quasi-degenerate states.
- [53] P. Sierant and J. Zakrzewski, New J. Phys. **20**, 043032 (2018).
- [54] P. Prelovsek, J. Bonca, Strongly Correlated Systems: Numerical Methods, vol. 176, Springer, 2013.
- [55] S. R. Manmana, A. Muramatsu, and R. M. Noack, AIP Conf. Proc. **789**, 269 (2005).
- [56] N. Mohankumar and S. M. Auerbach, Comput. Phys. Commun. **175**, 473 (2006).
- [57] We thank the authors of ref [11] for the release of their code on GitHub, which was used in [11].
- [58] T. Zhang and G.-B. Jo, Sci. Rep. **5**, 16044 (2015).
- [59] S. Taie, H. Ozawa, T. Ichinose, T. Nishio, S. Nakajima, and Y. Takahashi, Sci. Adv. **1** (2015), 10.1126/sciadv.1500854.
- [60] S. Mukherjee, A. Spracklen, D. Choudhury, N. Goldman, P. Ohberg, E. Andersson, and R. R. Thomson, Phys. Rev. Lett. **114**, 245504 (2015).
- [61] R. A. Vicencio, C. Cantillano, L. Morales-Inostroza, B. Real, C. Meja-Cortès, S. Weimann, A. Szameit, and M. I. Molina, Phys. Rev. Lett. **114**, 245503 (2015).

## Supplemental Material

### I. System-size dependence in level spacing analysis

In the level spacing analysis (LSA), the results slightly depend on the system size. In our numerical simulation, the system size is limited to  $L = 16$ , and  $N = 4$  (filling  $1/8$  case). In the LSA, as mentioned in the main text, we employ the unfolding method to obtain a clear probability distribution. As a specific example, we show the system-size dependence for the non-interacting flat-band case, as presented in Fig. A1 (a). For the  $L = 8$  case, the shape of the probability distribution is different from that of the Poisson distribution. The value of  $P(s)$  near  $s \sim 0$  tends to increase for a small system size. On increasing the system size up to  $L = 16$ , the shape of the probability distribution is reasonably Poisson-like. Based on this tendency, we expect that for larger system sizes, the probability distribution approaches the exact Poisson distribution. Therefore, for the non-interacting flat-band system, the AL is expected to be clearly observed for a large system size. Such a system-size dependence is also exhibited for the interacting case. Figure A1 (b) shows the system-size dependence of the LSA for the  $V = 1$  case. Compared with the non-interacting case, the increasing tendency of  $P(s)$  in the vicinity of  $s \sim 0$  in small systems is weak. However, the probability distribution deviates from the exact Poisson distribution. On increasing the system size up to  $L = 16$ , the probability distribution approaches the Poisson distribution.

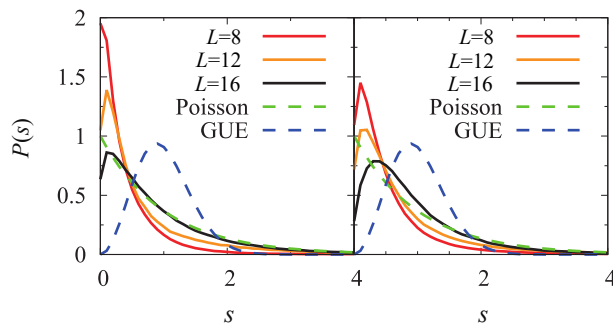


FIG. A1: System-size dependence of the level spacing analysis: (a) non-interacting flat-band case with  $\mu = 1$ . (b) interacting flat-band case with  $\mu = 1$ . In both the cases, the level spacing distribution,  $P(s)$ , approaches the Poisson distribution as the system size is increased.

### II. Dynamical properties of the Creutz ladder with strong disorders

As shown in Fig. 4 (c) in the main text, we studied the time evolution of a density-wave type configuration in the weak-disorder regime,  $\mu \leq 1$ . Here, we consider the strong-disorder regime for the interacting flat-band case.

As shown in the calculations of the LSA and IPR in the main text, a GUE-like behavior is observed at moderate disorder strengths, such as  $\mu \sim 6$ . For a stronger disorder regime, the probability distribution in the LSA returns to being the Poisson distribution, where the conventional disorder-induced AL or MBL is expected to occur. By using the Krylov subspace method explained in the main text, we calculated the dynamics of the particle imbalance,  $I(t)$ , defined in Eq. (4) in the main text. Figure A2 shows the results of the time evolution of  $I(t)$  in a strong-disorder system with  $V = 1$  for  $L = 12$ ,  $N = 3$ . The results are in good agreement with those of the LSA and IPR presented in the main text. For the  $\mu = 6$  case, the LSA exhibits a GUE-like distribution probability. Here, the calculation of  $\mu = 6$ , as displayed in Fig. A2, shows that  $I(t)$  decreases to a vanishingly small value in a long evolution. Contrastingly, the  $\mu = 30$  result indicates that the particle imbalance remains finite even in a long time evolution. This behavior corresponds to conventional MBL dynamics induced by disorder and consistent with the results of both the LSA and IPR calculations.

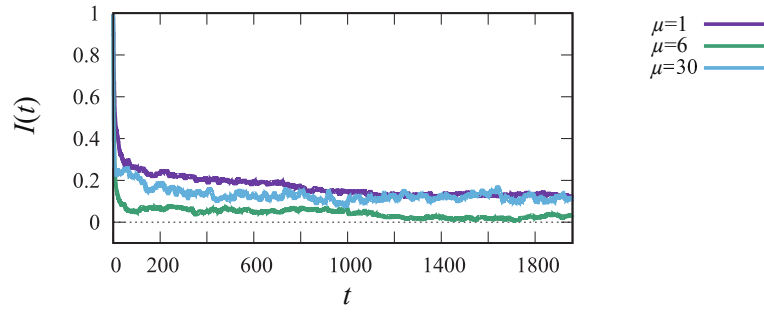


FIG. A2: Time evolution of the imbalance,  $I(t)$ , for  $\mu = 1, 6$  and  $30$  in the flat-band system with  $V = 1$ . Interestingly,  $I(t)$  for  $\mu = 6$  decreases to a vanishingly small value, whereas  $I(t)$  for  $\mu = 6$  and  $30$  remains finite. This behavior is in good agreement with the results of the LSA and IPR, which indicate the existence of a crossover at  $\mu \sim 6$ ,  $L = 12$ , and  $N = 3$ . We averaged the calculations over 50 disordered samples.